LASER SURFACE ENGINEERING OF METALLIC COMPONENTS

J. Dutta Majumdar and I. Manna
Department of Metallurgical and Materials Engineering,
Indian Institute of Technology, Kharagpur-721302, India

ABSTRACT

The engineering solution to improve the surface dependent properties like wear, corrosion and oxidation resistance involves tailoring the surface composition and/or microstructure of the near-surface region of a component without affecting the bulk. This may be achieved, using a high power laser beam as a source of heat, by surface hardening, melting, alloying and cladding. Fast heating/cooling rate (10^4–10^{11} K/s), very high thermal gradient (10^6–10^8 K/m) and ultra-rapid resolidification velocity (1-30 m/s) are the characteristics of this process which often develop exotic microstructures and compositions having large extension of solid solubility and metastable or even amorphous phases in the surface. This paper gives a brief review of the present status and future scope of laser assisted surface engineering with particular reference to the authors' work.

INTRODUCTION

Failure of engineering materials due to corrosion, oxidation, friction, fatigue and wear/abrasion is most likely to initiate from the surface because: (i) free surface is more prone to environmental degradation, and (ii) intensity of externally applied load is often highest at the surface [1]. The engineering solution to minimize or eliminate such surface initiated failure lies in tailoring the surface composition and/or microstructure of the near surface region of a component without affecting the bulk [1-5]. In this regard, the more commonly practiced conventional surface engineering techniques like galvanizing, diffusion coating, carburizing, nitriding and flame/induction hardening possess several limitations like high time/energy/material consumption, poor precision and flexibility, lack in scope of automation/ improvisation and requirement of complex heat treatment schedule. Furthermore, the respective thermodynamic and kinetic constraints of restricted solid solubility limit and slow solid state diffusivity impose additional limitations of these conventional or near-equilibrium processes [6,7].

In contrast, the surface engineering methods based on application of electron, ion and laser beams are free from these limitations. A directed energy electron beam is capable of intense heating due to laser-matter interaction (as shown in Fig.1)and melting of the surface of most refractory metals and ceramics [7]. However, the energy deposition profile in the irradiated zone under electron beam is gaussian

(as shown in Fig.2), and hence, the latter is more suitable for deep penetration welding or cladding of similar or dissimilar solids [7]. Moreover, the scope of generation of x-ray by rapid deceleration of high-energy electrons impinging on a solid substrate poses additional disadvantage of a possible health hazard. As an alternative, ion beam processing offers practically an unlimited choice and flexibility of tailoring the surface microstructure and composition with an implant which has otherwise no or very restricted solid solubility in a given substrate [8,9]. However, the peak concentration of implanted species, like the energy deposition peak in electron beam irradiation, lies underneath and does not coincide with the surface [7]. Furthermore, the requirements of an expensive ionization chamber, beam delivery system and ultra-high vacuum level are serious impediments against large-scale commercial exploitation of ion beam assisted surface engineering methods. In comparison, laser circumvents majority of the limitations cited above with regards to both conventional and electron/ion beam assisted surface engineering methods and offers a unique set of advantages in terms of economy, precision, flexibility and novelty of processing and improvement in surface dependent properties [6,7,10-12].

Among the notable advantages, laser surface engineering (LSE) enables delivery of a controlled quantum of energy (1-30 J/cm^2) or power density (10^4-10^7 W/cm^2) with precise temporal and spatial distribution either in short pulses (10^{-3} to 10^{-12} s) or as a continuous wave (CW). The process is characterized by an extremely fast heating/cooling rate (10^4-10^{11} K/s), very high thermal gradient (10^6-10^8 K/m) and ultra-rapid resolidification velocity (1-30 m/s) [1,4,5]. These extreme processing conditions very often develop an exotic microstructure and composition in the near surface region with large extension of solid solubility and formation of metastable or even amorphous phases.

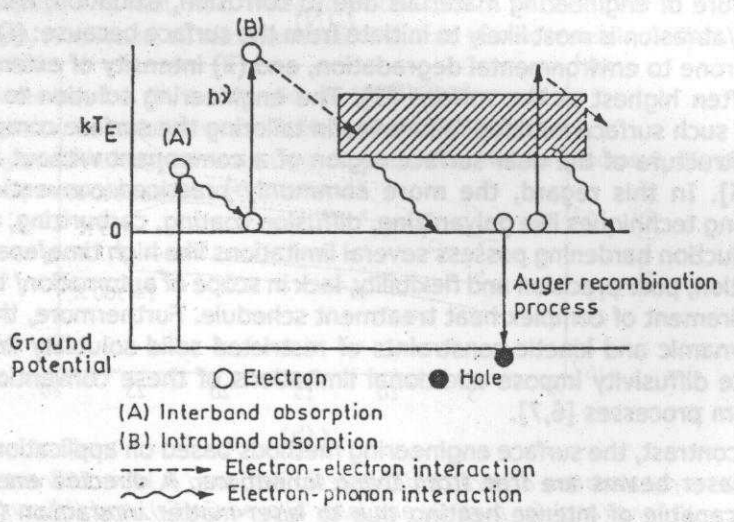

Fig. 1 : Schematic diagram depicting electron excitation and carrier relaxation process in materials subjected to intense laser irradiation.

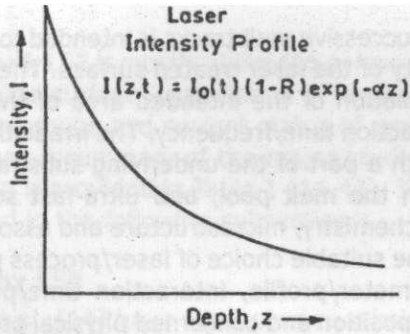

Fig. 2 : Spatial profile of deposited energy following laser irradiation of solid matter.

LASER SURFACE ENGINEERING

Fig. 3 presents a brief classification of different LSE methods that involve mainly two types of processes. The first type is meant for only microstructural modification of the surface without any change in composition (hardening, melting, remelting, shocking, texturing and annealing), while the other requires both microstructural as well as compositional modification of the near-surface region (alloying, cladding, etc.).

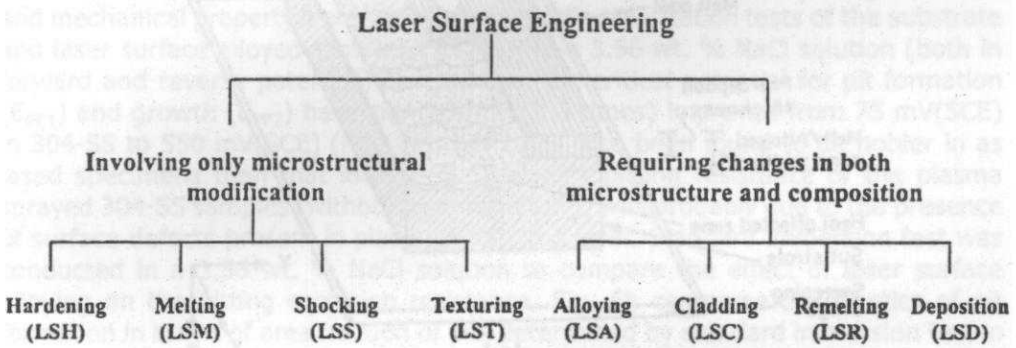

Fig. 3 : General classification of laser surface engineering.

Among the various LSE methods, laser surface alloying (LSA) involves melting of a deposited layer along with a part of the underlying substrate to form an alloyed zone for improvement of wear, corrosion and oxidation resistance. Fig. 4a illustrates the scheme of LSA with a continuous wave laser. It includes three major parts: a laser source with a beam focusing and delivery system, a lasing chamber with controlled atmosphere and a microprocessor controlled sweeping stage where the specimen is mounted for lasing. The process includes melting, intermixing and rapid solidification of a thin surface layer with pre/co- deposited alloying elements (Fig. 4b). The coating material may be pre-deposited by any of the conventional means like electro-deposition, plasma spray and physical/chemical vapor deposition or may be injected in the form of powder or powder mixture into the melt at the time of laser treatment and is termed as co-deposition. In LSA with a pre- or co-deposition,

a 20-30 % overlap of the successive melt tracks is intended to ensure microstructural/ compositional homogeneity of the laser treated surface. The sweeping stage (x-y or x-y-z-θ) allows laser irradiation of the intended area of the sample-surface at an appropriate rate and interaction time/frequency. The irradiation results into transient melting of the deposit with a part of the underlying substrate, rapid mass transfer by diffusion/convection in the melt pool, and ultra-fast solidification to form an alloyed zone. The depth, chemistry, microstructure and associated properties of the alloyed zone depend on the suitable choice of laser/process parameters i.e. incident power/energy, beam diameter/profile, interaction time/pulse width, pre or co-deposition thickness/ composition and concerned physical properties like reflectivity, absorption coefficient, thermal conductivity, melting point and density.

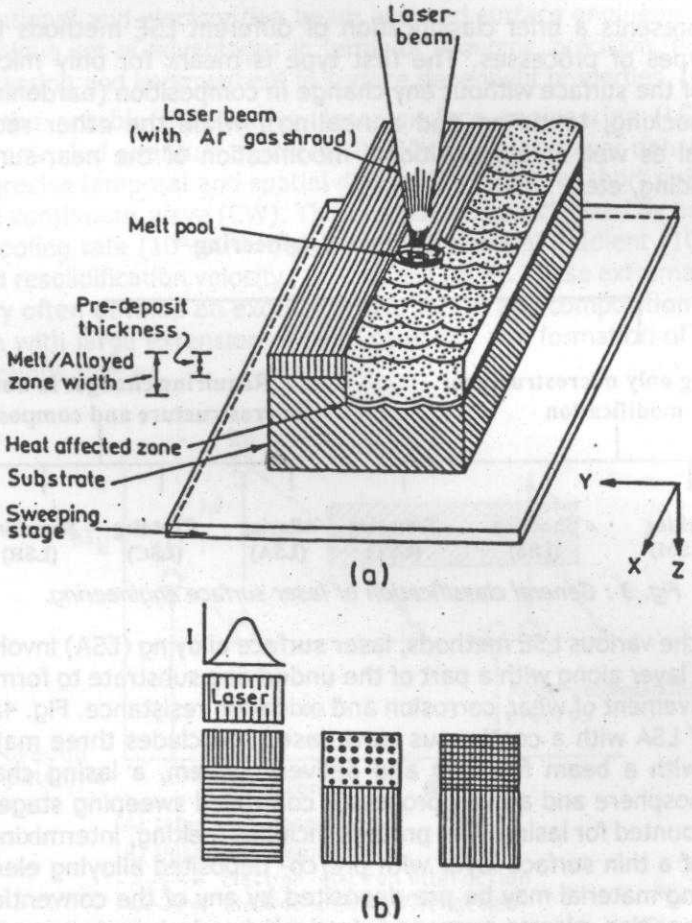

Fig. 4 : (a) Schematic hardware set up for laser surface alloying (LSA), (b) the processes of heating/melting, intermixing and solidification in LSA.

LSE of Ferrous Alloys

As already mentioned, LSE is mostly utilized to enhance resistance to corrosion, oxidation, wear and similar surface degradation of engineering materials. In this section, we will review the scope and current status of understanding about LSE of Fe-based or ferrous alloys. A summary of the major studies carried out in the last few years in this direction is provided in Table 1 [14-44]. The significant findings of the authors are discussed in the following subsections:

Corrosion resistance by LSE

Parvathavarthini et al. [14] have attempted to eliminate the susceptibility to inter-granular corrosion of the cold worked and sensitized AISI 316 stainless steel by laser surface melting (LSM). Similarly, LSM in nitrogen atmosphere or of nitrogen bearing steel is reported to improve the resistance to pitting corrosion of AISI 304 stainless steel [14,15]. In either case, this improvement may arise due to the presence of chromic oxide and nitrogen compound on the surface and consequent reconstruction of the passive layer or barrier to the electrolyte.

Dutta Majumdar and Manna [21] have investigated the effect of LSM and LSA of plasma spray deposited Mo on AISI 304 stainless steel (304-SS). Fig. 5 shows the optimum conditions (shaded region) for the formation of a homogeneous microstructure and composition in this study for improvement in pitting corrosion and mechanical property. Potentiodynamic anodic polarization tests of the substrate and laser surface alloyed samples (SS(Mo)) in a 3.56 wt. % NaCl solution (both in forward and reverse potential) showed that the critical potential for pit formation (E_{PP1}) and growth (E_{PP2}) have significantly (2-3 times) improved from 75 mV(SCE) in 304-SS to 550 mV(SCE) (Fig. 6a). EPP2 has also been found to be nobler in as lased specimens than that in 304-SS. The poor pitting resistance of the plasma sprayed 304-SS samples (without laser remelting) was probably due to the presence of surface defects present in plasma deposited layer. Standard immersion test was conducted in a 3.56 wt. % NaCl solution to compare the effect of laser surface alloying on the pitting corrosion resistance. Fig. 6b compares the kinetics of pit formation in terms of area fraction of pits determined by standard immersion test in a 3.56 wt.% NaCl solution as a function of time (t) between 304-SS and SS(Mo) lased with 1210 MW/m^2 power density and 31.7 mm/s scan speed for deposit thickness of 250 μm (corresponding to highest E_{PP1}). It is evident that both the extent and rate of pitting were significantly reduced in the SS(Mo) as compared to that in 304-SS. Furthermore, the process of pitting in 304-SS follows a sigmoidal nature marked by a substantially rapid initial stage than that of the later stage with no incubation time. In comparison, pits were noticed in SS(Mo) only after 50 h of immersion, and the number increases linearly following a much slower kinetics as compared to that in 304-SS. Continuous circulation of the samples at 750 rpm for 10 to 75 h in a medium containing 20 wt. % sand in 3.56 wt. % NaCl solution showed a significant decrease in the kinetics of erosive-corrosion loss in SS(Mo) than that in 304-SS (Fig. 7). It was thus concluded that LSA is capable of imparting an excellent superficial microhardness and resistance to corrosion and erosion-corrosion properties to 304-SS due to Mo both in solid solution and as precipitates.

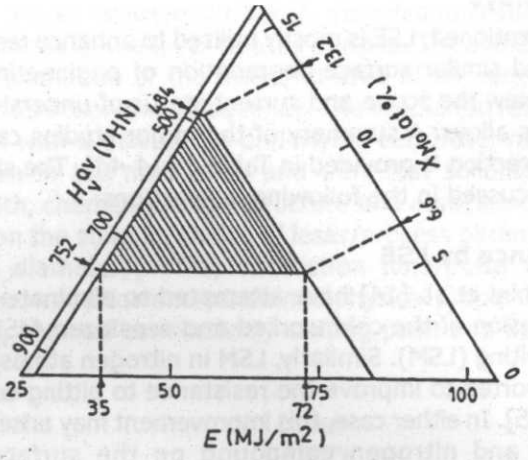

Fig. 5 : Process optimization diagram for selecting the necessary energy density (E) for laser surface alloying of 304-SS with Mo to achieve the desired composition (XMo) and hardness ( ) in the alloyed zone (shaded region).

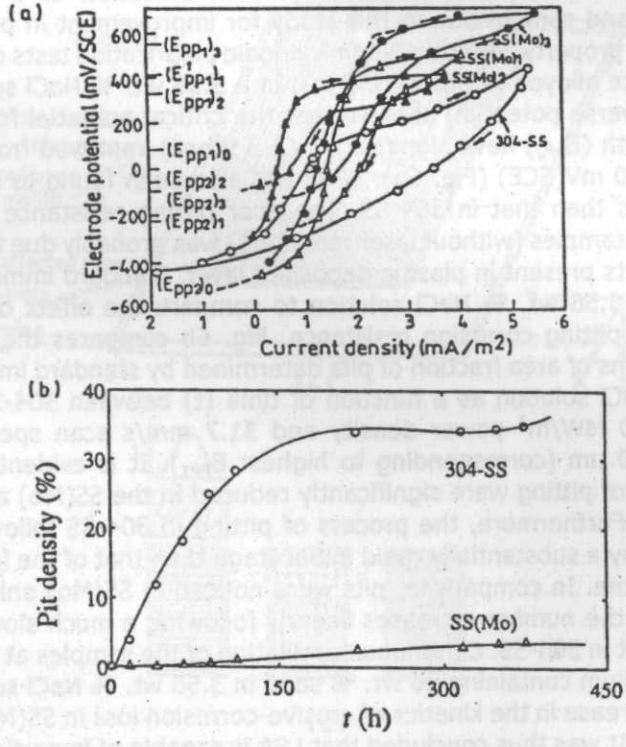

Fig. 6 : (a) cyclic potentiodynamic polarization behavior of 304-SS and laser surface alloyed of 304-SS with Mo in a 3.56 wt. % NaCl solution and (b) variation of pit density in 304-SS and SS(Mo) as a function of time (t) in a 3.56 wt. % NaCl solution.

Table 1 : Summary of selected studies on laser surface engineering of materials in the last few years (1999 onwards)

System	Year	LSE	Property	Scope	Results	Reference
I. LSE of Ferous Alloys						
Corrosion Properties						
AISI 316 stainless steel	2001	LSM	Corrosion	Improve intergrannular corrosion and intergrannular stress corrosion	LSM is effective in de-sensitization	Parvathavarthini et al. [14]
AISI 304 stainless steel	2001	LSM	Pitting	Role of LSM in N_2 or Ar atmosphere in enhancing pitting corrosion resistance	Technology for pitting decreases due to dissolution of nitrogen and formation of nitrides	Conde et al. [15]
AISI 1040 (NiCoCrB)	2001	LSA	Corrosion, Erosion	Improve both corrosion and erosion by LSA	corrosion resistance improves in mild steel but deteriorates in stainless steel. Both benefits are simultaneously impossible	Kwok et al. [16]
17-4 PH stainless steel	2001	LSAn	Fatigue, Stress corrosion	Reduce tendency for fatigue crack growth and stress corrosion cracking	Laser annealing produces duplex microstructure that retards crack growth in quasi-cleavage fracture	Tsay et al. [17]
G 10380 steel G 41400 martensite AISI 316L austenitic	2000	LSS	Corrosion, Stress corrosion	Introduce compressive residual stress and supress crack growth by laser assisted shot peening	Corrosion current decreases in martensitic steel. Laser peening is more effective in reducing stress corrosion	Peyer et al. [18]
UNS-S31603 austenitic stainless steel (Co,Ni,Mn,Cr,Mo)	2000	LSA	Corrosion, Erosion	Improve both corrosion and cavitation erosion corrosion by LSA	Resistance to erosion improves due to dispersed ceramic/ intermetallic phase but pitting resistance decreases	Kwok et al. [19]
AISI 304 stainless steel	2000	LSA	Corrosion	Investigate the role of Si in improving corrosion resistance	Si turns the matrix ferric andsegregates. Post LSA homogenization improves corrosion resistance	Isshiki et al. [20]
AISI 304 stainless steel (Mo)	1999	LSA	Pitting, Erosion	Attain AISI 316-SS equivalent corrosion property on 304-SS	Mo improves pitting and erosion corrosion resistanceof 304-SS	Dutta Majumdar and Manna [21]

Oxidation Properties						
Steel (Al)	2001	LSA	Oxidation	Improve oxidation resistance by LSA with predeposited Al	LSA with Al forms several Aluminides that imparts good oxidation resistance at 600°C up to 200 h.	Pillai et al. [22]
Stainless Steel	2000	LC	Cleaning	Remove oxide layers by laser assisted vaporization	Thin oxide layers could be removed irrespective of chemical composition and history in a narrow energy band	Psyllaki and Oltra [23]
Plain Carbon Steel (TiB_2)	2000	LSA	High temperature oxidation	Impart oxidation resistance by alloying with borides	Complex oxide layers develop on steel surface exposed to 600-1000°C following parabolic growth rate	Agarwal et al. [24]
Wear Properties						
S 31603 stainless steel (CrB_2, Cr_3C_2) SiC, TiC, WC, Cr_2O_3	2001	LSA	Cavitation erosion resistance	Enhance erosion resistance by developing a ceramic dispersed composite surface layer	Erosion resistance improves considerably for all carbides and borides except Cr_2O_3	Cheng et al. [25]
Austenitic stainless steel (Nano-Zr)	2000	LSA	Hardness, Erosion	Develop amorphous dispersed composite layer to improve resistance to erosion and wear	Hardness and wear/erosion resistance improves significantly due to dispersion of Zr-rich amorphous phase	Wu and Hong [26]
Austempered ductile iron (Cr)	2001	LSA LSH	Hardness, Wear	Improve adhesive/abrasive wear resistance of austempered ductile iron by LSA or LSH	LSH (thanLSA) is more effective in improving wear resistance and developing compressive residual stress	Roy and Manna [27]
AISI 1040 (TiB_2)	2000	LSA	Tribology, Wear	Develope boride coated/dispersed surface layer and improve wear resistance of low-carbon steel	LSA improves resistance to adhesive/abrasive wear and reduces friction coefficient	Agarwal and Dahotre [28]
Mild Steel (FeCr-TiC)	2000	LSR, SHS	Wear	Utilize SHS and LSR to develop a TiC dispersed surface composite	LSR homogenizes the microstructure and improves wear resistance	Tondu et al. [29]

Mild Steel (Hadfield, Fe-Mn-C)	1999	LSC	Wear	Improve hardness, wear and bulk mechanical properties	LSC improves wear resistance and bulk mechanical properties of the clad	Pelletier et al. [30]
II LSE of Superalloys and Special Steels						
Cr-Mo Steel (Cr)	2000	LSA	Oxidation	Improve high temperature oxidation resistance	LSA enhances oxidation resistance in 800-1000°C due to Cr_2O_3 rich scale	Manna et al. [31]
Martensitic steel (Ni-alloy)	1999	LSC	Hardness, Wear	Improve wear and erosion resistance of the base steel	LSC significantly increased hardness and erosion resistance	Zhang et al. [32]
III. LSE of Non-Ferrous Alloys						
Al and its alloys - Corrosion properties						
Al-6013 + SiC_p Composite	1999	LSM	Corrosion	Improve pitting and general corrosion properties by LSM	Rapid solodification of LSM refines the surface microstructure and improves the corrosion resistance	Yue et al. [32]
Al and its alloys - Oxidation properties						
6061 Al alloy (Al + TiC)	2001	LSC LSA	Oxidation	Improve oxidation resistance of Al-alloy by LSC/LSA	TiC+Al composite coating improves oxidation resistance in 200-600°C	Katipelli and Dahotre [34]
Al and its alloys - Wear properties						
Al + SiC	1999	LSS	Hardness, Wear	Improve oscillating wear property by LSS of HVOF coated composite surface layer	Both hardness and wear resistance improve by LSS due to residual compressive stress	Schinck et al. [35]
Al (Al_3Ti)	1999	LSC	Wear	Improve wear resistance	Composite intermetallic layer on surface enhances wear resistance	Uenishi and Kobayashi [35]

Cu and its alloys						
Cu-Cr-Fe	2000	LSR	Hardness, Wear	Improve tribological properties of powder compacts by LSR	LSR improves hardness and wear resistance and reduces friction	Geng et al. [37]
Cu (Cr)	1999	LSA	Wear, Erosion	Improve wear/erosion resistance of Cu by LSA with Cr	LSA enhances resistance to adhesive/abrasive wear and erosion due to solid solution and dispersion hardening	Dutta Majumdar and Manna [38]
Mg and its alloys						
Mg+SiC (Al-Si)	2001	LSC	Corrosion	Improve corrosion resistance by LSC with Al+Si alloy	LSC improves corrosion resistance LSC parameters have strong influence	Wang and Yue [39]
AZ91D and AM60B Mg alloys	2001	LSM	Corrosion	Improve corrosion resistance by LSM	Uniform and refined microstructure improves corrosion resistance	Dube et al. [40]
AZ91 Mg alloy	1999	LSM	Corrosion	Enhance corrosion resistance	Pulsed excimer laser irradiation improves corrosion resistance	Schippman et al. [41]
MEZ, Mg alloy	2002	LSA	Wear and Corrosion	Enhance wear and corrosion resistance	Laser parameters have influence on wear resistance	J. Dutta Majumdar et al. [42]
Ti and its alloys						
Ti (Si,Al,Si+Al)	2000	LSA	Wear, Friction	Improve wear resistance by LSA	LSA with Si is more effective than Al/Si+Al to improve wear resistance	J. Dutta Majumdar et al. [43]
Ti (Si,Al,Si+Al)	1999	LSA	Cyclic oxidation	Improve oxidation resistance by LSA with Si/Al	LSA with Si/Si+Al is more effective than Al in enhancing cyclic oxidation resistance between ambience/750°C	J. Dutta Majumdar et al. [44]

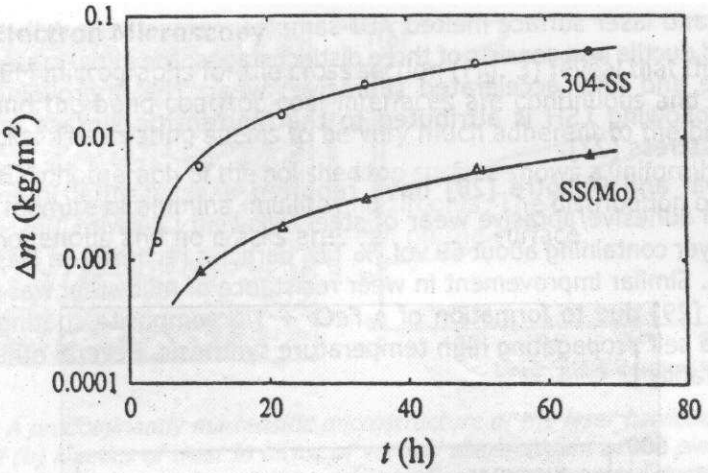

Fig. 7 : Comparison of material loss per unit area (Δm) due to erosion as a function of t for 304-SS and laser surface alloyed of 304-SS with Mo in a mixture of 20% sand in 3.56 wt. % NaCl solution [21].

Oxidation resistance by LSE

Oxidation is another serious mode of surface degradation that gets aggravated under unabated counter ionic transport of cations and anions at elevated temperature. In the past, several attempts have been made to enhance resistance to oxidation by LSA, LSC and similar LSE techniques [22-24]. Manna et al. [31] attempted to enhance the high temperature oxidation resistance (above 873 K) of 2.25Cr-1Mo ferritic steel by laser surface alloying (LSA) with co-deposited Cr using a 6 kW continuous wave CO_2 laser. The main process variables chosen for optimizing the LSA routine were laser power (from 2 to 4 kW), scan speed of the sample-stage (150 to 400 mm/min) and powder feed rate (16 to 20 mg/s). Isothermal oxidation studies in air by thermogravimetric analysis at 973 and 1073 K for up to 150 h revealed that LSA had significantly enhanced the oxidation resistance of ferritic steel during exposure to 973 and 1073 K (Figs. 8a,b). Post oxidation microstructural analysis suggests that an adherent and continuous Cr_2O_3 layer is responsible for the improvement in oxidation resistance [31].

Wear resistance by LSE

Attempt to improve wear resistance of steel by LSE seems to be more effective than the attempts to enhance the resistance to corrosion and oxidation. Cheng et al. [25] have added a mixture of WC-Cr_3C_2-SiC-TiC-CrB_2 and Cr_2O_3 to produce a metal matrix composite surface on stainless steel UNS-S31603. Following LSM, cavitation erosion resistance improved in all cases except for Cr_2O_3. Roy and Manna [27] have demonstrated that laser surface hardening (LSH), instead of LSA or LSM is more effective in enhancing hardness and wear resistance of unalloyed austempered ductile iron (ADI). Figs. 9a,b show the typical martensitic microstructure developed by LSH and significant improvement in adhesive wear of laser hardened vis-à-vis

as-received and laser surface melted ADI samples, respectively. Adhesive wear of austempered ductile iron consists of three distinct stages: the initial rapid, subsequent steady state and final accelerated (abrasive) wear. The improvement in wear resistance following LSH is attributed to the martensitic surface with residual compressive stress [27].

Agarwal and Dahotre [28] have reported a substantial improvement in resistance to adhesive/abrasive wear of steel following LSA with T_iB_2. The surface composite layer containing about 69 vol. % T_iB_2 particles recorded an elastic modulus of 477.3 GPa. Similar improvement in wear resistance of mild steel was reported by Tondu et al. [29] due to formation of a FeCr + TiC composite coating formed by laser assisted self propagating high temperature synthesis. Several other examples are cited in Table 1.

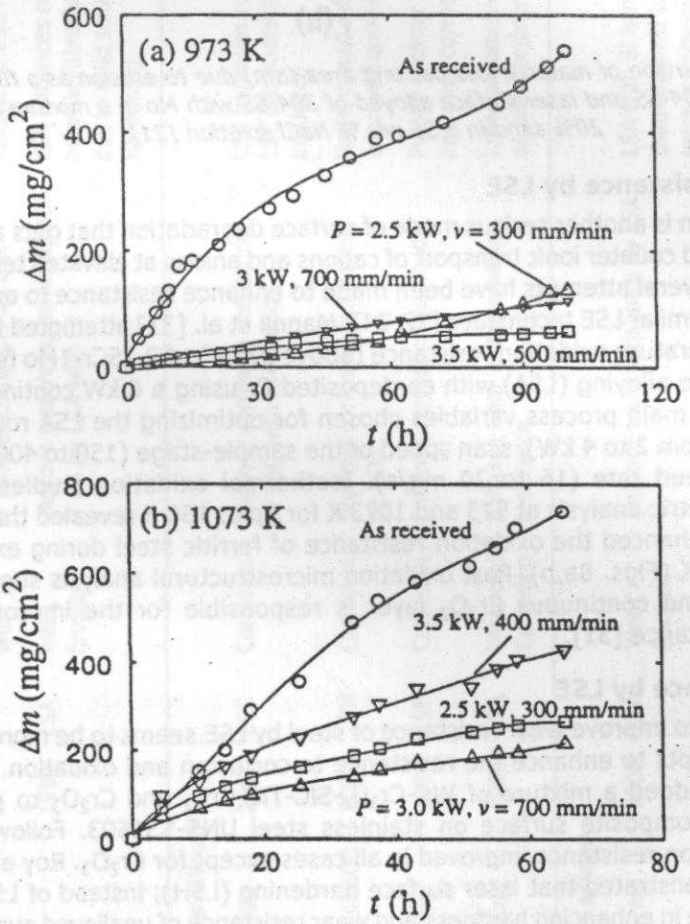

Fig. 8 : Kinetics of isothermal oxidation of 2.25Cr-1Mo ferritic steel laser surface alloyed with Cr and exposed to (a) 973 and (b) 1073 K in air, respectively [31]

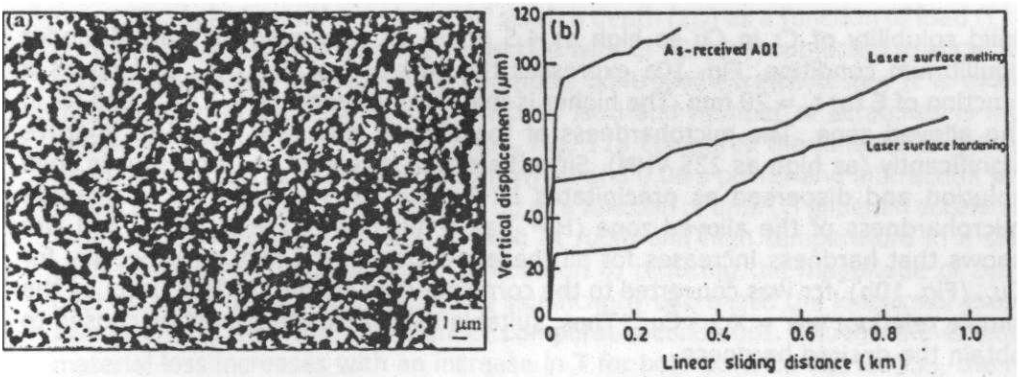

Fig. 9 : (a) A predominantly martensitic microstructure of the laser hardened sample surface, and (b) kinetics of wear in terms of vertical displacement of the pin-head as a function of sliding distance during adhesive wear testing of austempered ductile iron (ADI) subjected to LSM and LSH with a pin-on-disc machine in dry condition at 5 kg load. For details, please see [27,51].

LSE of Non-Ferrous Alloys

Surface dependent degradation by wear, oxidation and corrosion is as much a problem in nonferrous metals and alloys as that in ferrous alloys. Thus LSE in widely applied to Al, Ti, Cu, Mg and other important nonferrous metals and alloys to extend the service life of components subjected to severe conditions of wear, oxidation and corrosion. In this section, we will briefly review the scope and current status of understanding regarding the application of LSE to enhance surface dependent properties of non-ferrous alloys. For a ready reference, Table 1 summarizes the major work done in the recent past in this area [33-44].

Several attempts have been made to improve corrosion resistance of Al-based alloys by LSM [33], LSA [34] and LSC/LSR [36]. While grain refinement and microstructural homogeneity are responsible for better corrosion resistance in LSM dispersion of intermetallic and/or amorphous phases are considered crucial for corrosion resistance following LSC/LSR. Katipelli and Dahotre [34] have achieved considerable improvement in oxidation resistance of 6061 Al alloy by LSA with Al +TiC.

Improvement in wear resistance of Al alloys seems to necessitate addition of ceramic or intermetallic particles by LSC or LSA [35,36]. Usually, the alloyed or clad layer possesses a high hardness and consists of intermetallic or amorphous phases [35,36]. Schnick et al. [35] induced residual compressive stress by laser surface shocking and achieved a significant improvement in wear resistance in HVOF spray coated SiC on Al.

Manna and Dutta Majumdar [38] attempted to enhance the wear and erosion resistance of Cu by laser surface alloying with Cr (electrodeposited with 10 and 20 μm thickness, t_z). Total Cr content (Xcr), Cr in the form of precipitates (fcr) and Cr in solid solution with Cu (Cu_{cr}) were determined by energy dispersive spectrometry, optical microscope and X-ray diffraction technique, respectively. LSA extended the

solid solubility of Cr in Cu as high as 4.5 at. % as compared to 1 at. % under equilibrium condition. Fig. 10a expresses the variation of X_{cr}, Cu_{cr}, and fcr as a function of E for t_z = 20 mm. The higher is the E, the smaller the X_{cr}, Cu_{cr}, and fcr in the alloyed zone. The microhardness of the alloyed zone was found to improve significantly (as high as 225 VHN). Since hardness is related to Cr present in solid solution and dispersed as precipitates in the matrix, the variation of average microhardness of the alloyed zone (H_v^{av}) as a function of the X_{cr}, Cu_{cr}, and wcr shows that hardness increases for all these microstructural factors, especially for Cu_{cr} (Fig. 10b). fcr was converted to the corresponding weight fraction (wcr) by the simple relation: wcr = Xcr - Cu_{cr}. Thus, suitable LSA parameters must be chosen tp obtain the desired hardness.

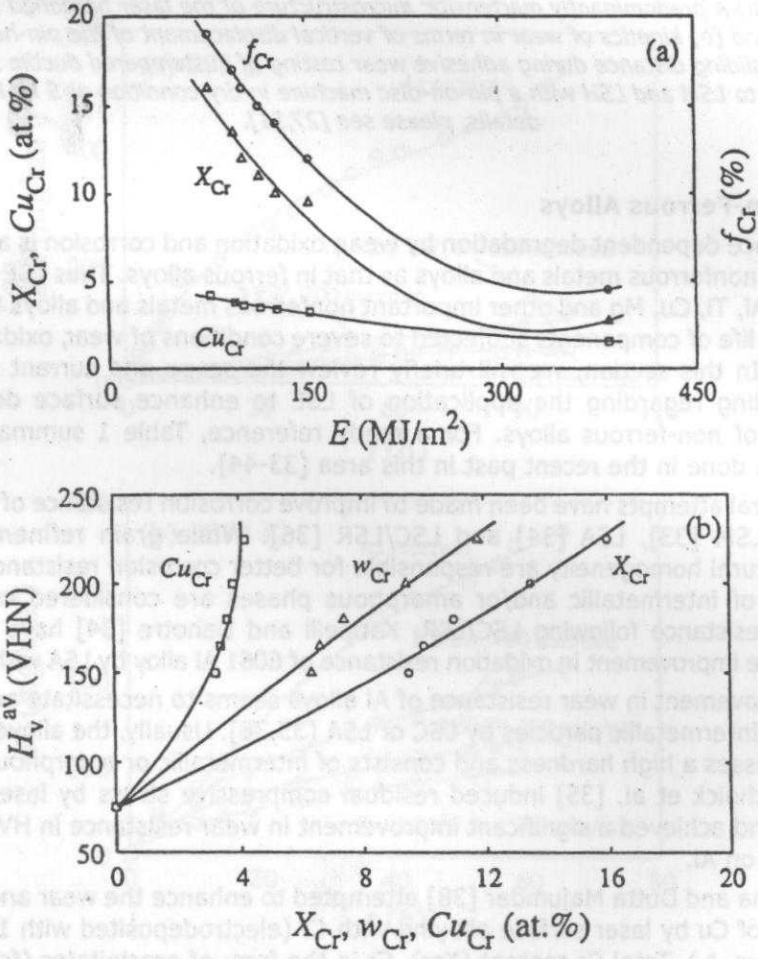

Fig. 10 : (a) Variation of Cr-content (X_{cr}), dissolved Cr in solid solution (Cu_{cr}) and volume fraction of Cr-precipitates (fcr) as a function of energy density (E), and (b) variation of as a function of X_{Cr}, Cu_{cr} and fcr. For details, please see [38].

Fig. 11a shows the variation of scratch depth (z_{sc}) as a function of load (L) for pure Cu as well as laser surface alloyed Cu with Cr [Cu(Cr)] subjected to scratching with an oscillating steel ball in a computer controlled scratch tester. It is evident that the rate of increase of z_{sc} with both load and number of scratches is much higher in pure Cu than that in Cu(Cr). Fig. 11b compares the kinetics of material loss (Δm) of Cu(Cr) lased with 1590 MW/m² and 0.08 s power and interaction time, respectively (t_z = 20 μm) with that of Cu as a function of time (t) under an accelerated erosive wear condition conducted both at room and high temperature in a slurry bath containing 20 wt. % sand. In addition to reducing the magnitude of Δm by over an order of magnitude, LSA has significantly decreased the kinetics of erosion loss in Cu(Cr) than that in Cu under comparable conditions. Though the extent of material loss increases with an increase in T for both pure Cu and Cu(Cr), the rate of erosion loss for Cu(Cr) is negligible as compared to a substantial change in Δm with T for pure Cu, especially beyond 370 K.

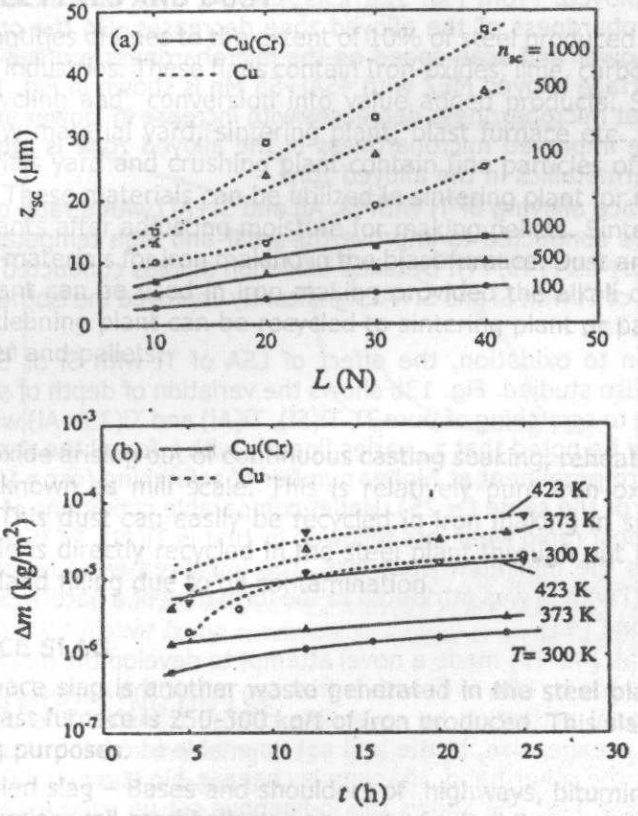

Fig. 11 : (a) Variation of scratch depth (zsc) with load (L) for different numbers of oscillations (nsc) for pure Cu and laser alloyed Cu(Cr), and (b) comparison between of material loss per unit area (Δm) due to erosion of Cu(Cr) and Cu as a function of time (t) at different temperature (T) due to erosion in flowing SiO2 dispersed oil medium. For details please see [134,195].

Uniform and refined surface microstructure by LSM seems quite effective in improving corrosion resistance in AZ91D/AM60B [40], AZ91 [41] and other commercial Mg-based alloys. Recently, Wang and Wue [39] have achieved significant improvement in corrosion resistance of SiC dispersed Mg by LSC with Al-12Si alloy layer. In this regard, Dutta Majumdar et al. [42] reported laser surface alloying of a magnesium alloy (MEZ) with 76Al+24Mn and 55Al+45Mn. Figs. 12a,b present the microhardness profiles for laser surface alloyed MEZ specimens with (a) 76Al+24Mn and (b) 45Al+55Mn (lased under different processing conditions) as a function of depth from the surface measured on the cross sectional plane. The microhardness of the alloyed zone has increased significantly to as high as 350 VHN as compared to 35 VHN of the as-received one. Moreover, for both the cases, the microhardness of the alloyed zone is maximum near the surface and gradually decreases away from the surface towards the interface. Gradual decrease in microhardness value is attributed to decrease in alloying content and volume fraction of intermetallic phases with depth. The microhardness of the alloyed zone was found to vary with the laser parameters employed. From Fig. 12a it is relevant that with increase in applied power, the microhardness of the alloyed zone decreases. On the other hand, the effect of laser power and scan speed on the microhardness profiles of the alloyed zone in laser surface alloyed MEZ with 45Al+55 Mn is shown in Fig. 12b. From Fig. 12b it is clear that microhardness decreases with increase in power and decrease in scan speed. The improved microhardness in the alloyed zone is attributed to the presence of intermetallics in the alloyed zone.

Laser surface alloying of Ti with Si, Al, and Si+Al (with a ratio of 3:1 and 1:3, respectively) was conducted to improve the wear and high temperature oxidation resistance of Ti by LSA (43,44). Detailed oxidation studies conducted at 873-1023K showed that LSA of Ti with Si and Si+Al significantly improved the isothermal oxidation resistance (Fig.13a).

In addition to oxidation, the effect of LSA of Ti with Si or Si+Al on wear resistance was also studied. Fig. 13b shows the variation of depth of scratching (z_w) with load (L) due to scratching of pure Ti, Ti(Si), Ti(Al) and Ti(3Si+Al) with a hardened steel ball. It may be noted that z_w varies linearly with L for all the cases. The effect of L on z_{sc} is more prominent at higher number of scratching (nsc > 1000) than that at a lower value of the same (= 25). Under comparable conditions of scratching, Ti undergoes the most rapid wear loss followed by that in Ti(Al), Ti(3Si+Al) and Ti(Si). Ti(Si) undergoes the minimum wear loss. The improved wear resistance of laser surface alloyed Ti with Si was attributed to the formation of a hard Ti_5Si_3 precipitates in the alloyed zone [43].

Manna et al. [45-47] made a novel attempt to develop the material for neural stimulation electrode by LSA of Ti with Ir that can mimic the normal spatio-temporal pattern of neuronal activation by reversible charge transfer. The usual electrode made of iridium is expensive, brittle and not amenable to miniaturization by plastic deformation. On the other hand, titanium is cheaper, bio compatible and amenable to drawing/etching. Fig. 14a shows the indigenous set up used for fabricating the electrode by LSA. Intelligent combination of laser parameters, powder composition and post LSA etching was used to develop the desired microstructure (Fig. 14b). Though charge density could not be measured due to exceedingly uneven surface intentionally developed by special etching (meant for increasing the surface area), the total charge was comparable to that of pure iridium in appropriate solution [47].

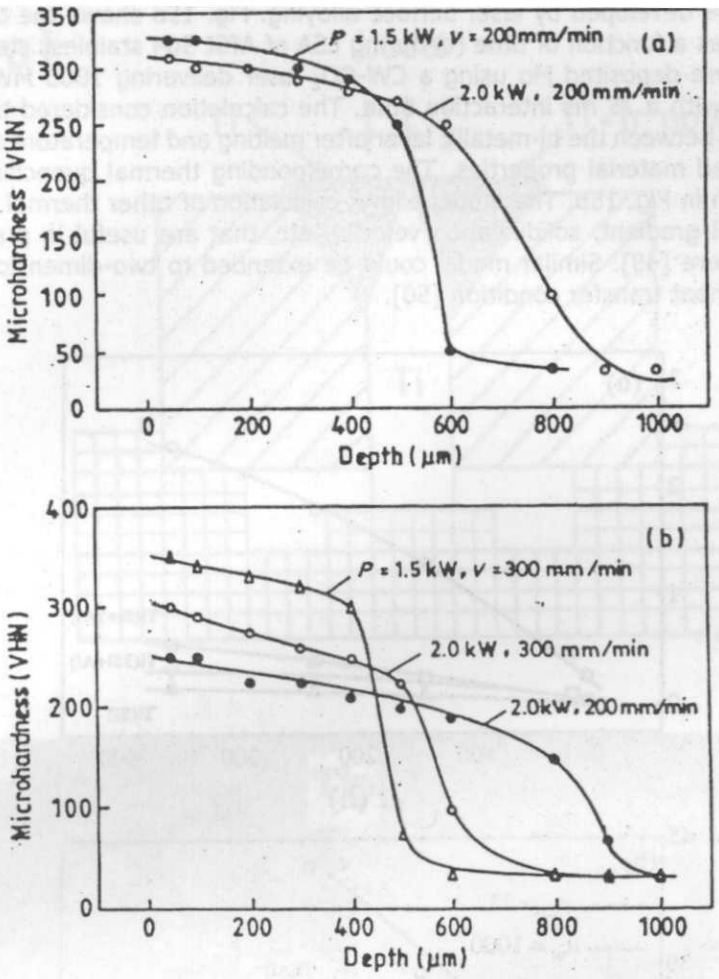

Fig. 12 : Microhardness profiles as a function of depth from the surface measured on the cross sectional plane in laser surface alloyed MEZ with (a) 76Al+24Mn and (b) 45Al+55Mn (processed under different lasing conditions as written in respective Figures).

MATHEMATICAL MODELING ON LSE

Studies on mathematical modeling of LSE mostly focus on predicting the thermal profile and composition in the laser irradiated volume. While the knowledge on thermal history and solute distribution is essential for predicting the properties, attempts have seldom been made to correlate the microstructure and property of the laser treated zone with the LSE parameters. Manna and Dutta Majumdar [48] developed a one dimensional heat transfer model based on explicit finite difference method to predict the thermal history (i.e. temperature profile, thermal gradient, cooling rate and solid-liquid interface velocity) and hence, the microstructure of the

alloyed zone developed by laser surface alloying. Fig. 15a shows the temperature (T) profile as a function of time (t) during LSA of AISI 304 stainless steel with 100 mm thick pre-deposited Mo using a CW-CO_2 laser delivering 1800 MW/m^2 power irradiation with a 25 ms interaction time. The calculation considered the effect of intermixing between the bi-metallic layer after melting and temperature dependence of concerned material properties. The corresponding thermal quenching rate has been shown in Fig. 15b. The model allows calculation of other thermal parameters like thermal gradient, solidification velocity, etc. that are useful in predicting the microstructure [49]. Similar model could be extended to two-dimensional radially symmetric heat transfer condition [50].

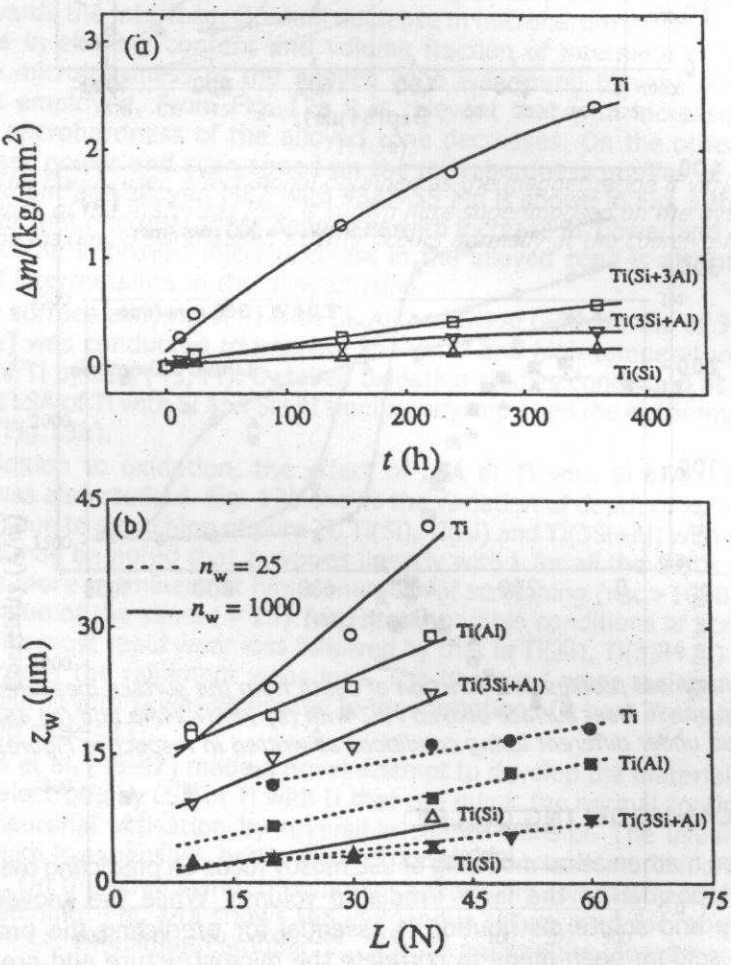

Fig. 13 : (a) kinetics of oxidation expressed as total weight gain per unit area (Δm) as a function of time (t), and (b) kinetics of wear in scratch test expressed as depth of scratch (zw) as a function of load (L) for as-received and laser surface alloyed Ti with Si, Al and Si+Al. For details about LSA, oxidation and wear test, please see [43,44].

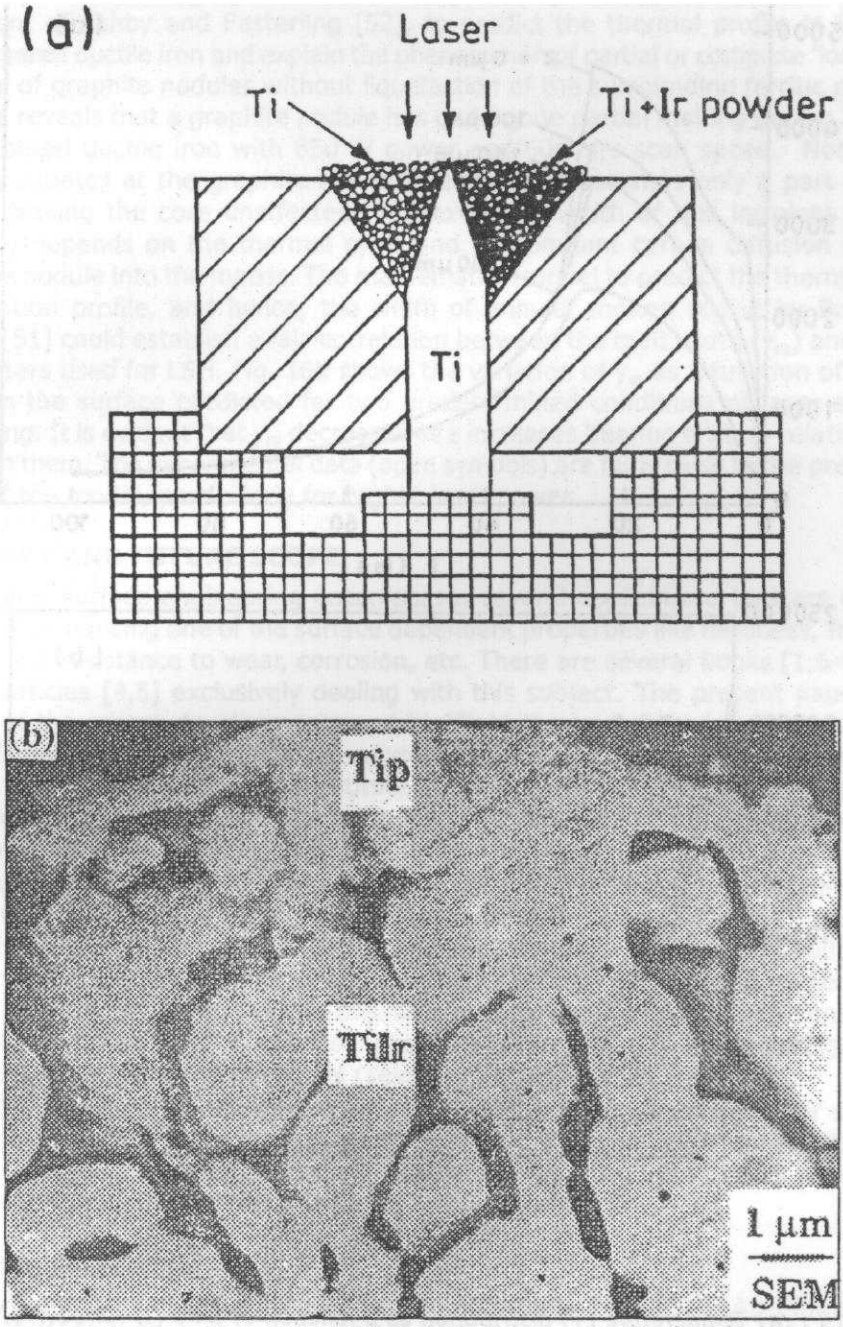

Fig. 14 : (a) Schematic diagram showing the set up used for LSA of Ti with Ir (or Ti+Ir) by CO2 laser pulse for developing neural stimulation electrode, and (b) microstructure of the alloyed zone showing a 3 fold increase in surface area following special etching [45,46]

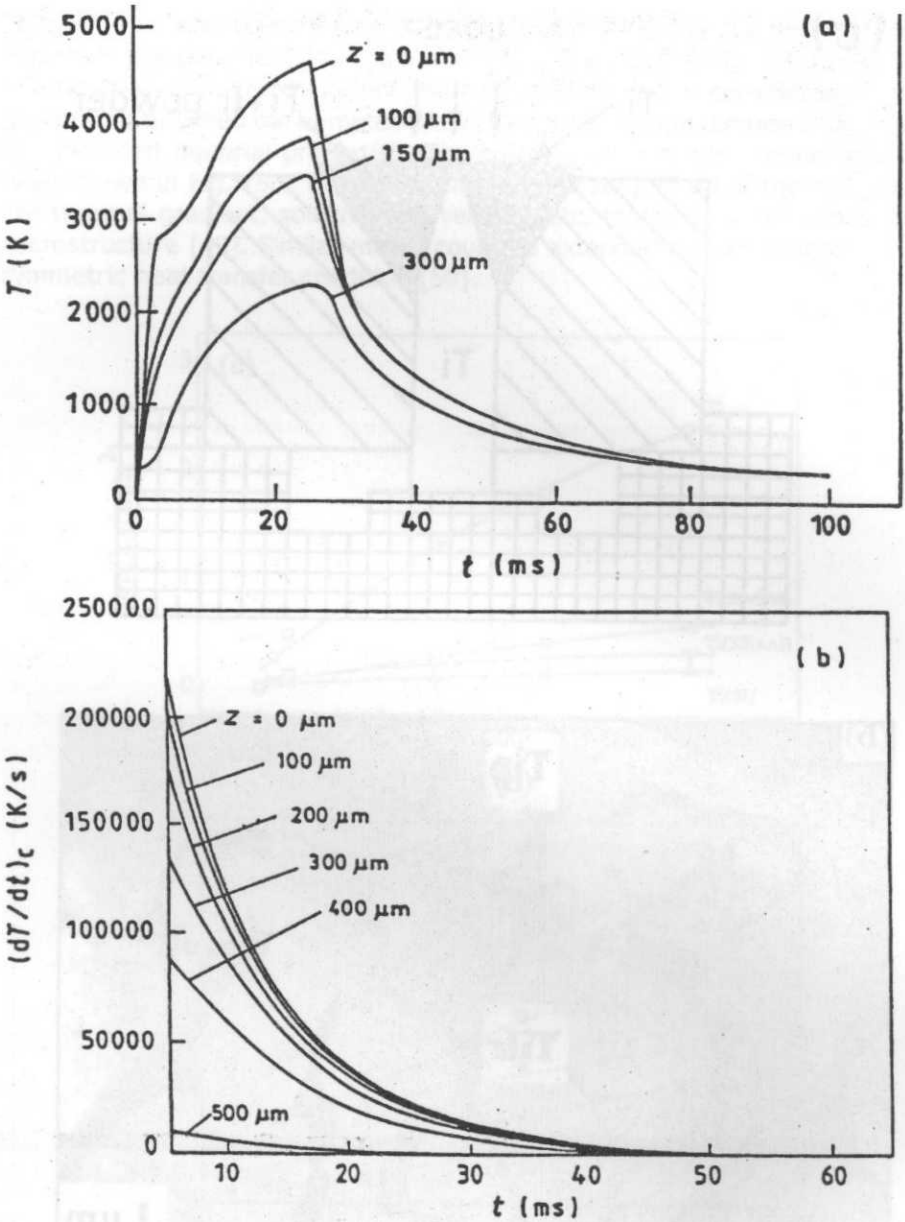

Fig. 15 : (a) Temperature (T) distribution as a function of time (t) for SS(Mo) at different levels of depth (z), and (b) variation of corresponding cooling rate (dT/dt)C as a function of time (t) at different z during LSA of AISI 304 stainless steel with Mo. For details, please see [49].

Roy and Manna [51] have used a simple analytical approach, based on the treatment of Ashby and Easterling [52], to predict the thermal profile in LSH of austempered ductile iron and explain the phenomenon of partial or complete 'localized melting' of graphite nodules without liquefaction of the surrounding ferritic matrix. Fig. 16a reveals that a graphite nodule has undergone partial melting during LSH of austempered ductile iron with 650 W power and 60mm/s scan speed. Note that melting initiates at the graphite-matrix interface and assumes only a part of the nodule leaving the core unaffected. The extent or width of this incipient fusion primarily depends on the thermal cycle and concomitant carbon diffusion profile from the nodule into the matrix. The mathematical model to predict the thermal and composition profile, and hence, the width of annular molten region by Roy and Manna [51] could establish a fair-correlation between the melt width (y_m) and laser parameters used for LSH. Fig. 16b shows the variation of y_m as a function of depth (z) from the surface predicted for two predetermined conditions of laser surface hardening. It is evident that y_m decreases as z increases bearing a linear relationship between them. The experimental data (open symbols) are fairly close to the predicted trend of the model, particularly for higher laser power.

SUMMARY AND FUTURE SCOPE

Laser surface engineering encompasses several applications that are mainly related to enhancing one of the surface dependent properties like hardness, friction, fatigue and resistance to wear, corrosion, etc. There are several books [1,6-8] and review articles [4,5] exclusively dealing with this subject. The present paper is a review of the recent developments and highlight the important issues concerning them. The current trend appears to suggest that the excimer and diode lasers with shorter wavelengths may soon substitute CO_2 even YAG lasers for LSE applications. Sustained efforts will then be needed to establish the microstructural evolution and scope of improvement following LSE with those new lasers.

Apart from structural applications, LSE could be useful in enhancing functional properties like magnetism, emission/absorption characteristics, sensors, microelectronic devices and several other applications requiring monolithic or functionally/ compositionally graded microstructures confined to smaller dimensions. The LSE processes described in this section are applicable to such functional application, provided the correct laser parameters (wavelength, mode, energy, etc.) are selected for the given materials (semiconductor, polymer, etc.).

The major outstanding issues concerning LSE are: (a) utilization of shorter wavelengths for more precise surface engineering, (b) developing compositionally and functionally graded microstructure, (c) elimination or minimization of structural/ coefficient mismatch and combining dissimilar materials.

ACKNOWLEDGEMENT

A major part of the work was carried out under the DST-DAAD-PPP project (INT/FRG/DAAD/M-115/99) of the DST, New Delhi. Partial financial support to JDM from the DST (Fast Track Scheme), ISIRD (IIT, Kharagpur), and to IM from the DST (SP/S2/K-17/98), New Delhi is gratefully acknowledged.

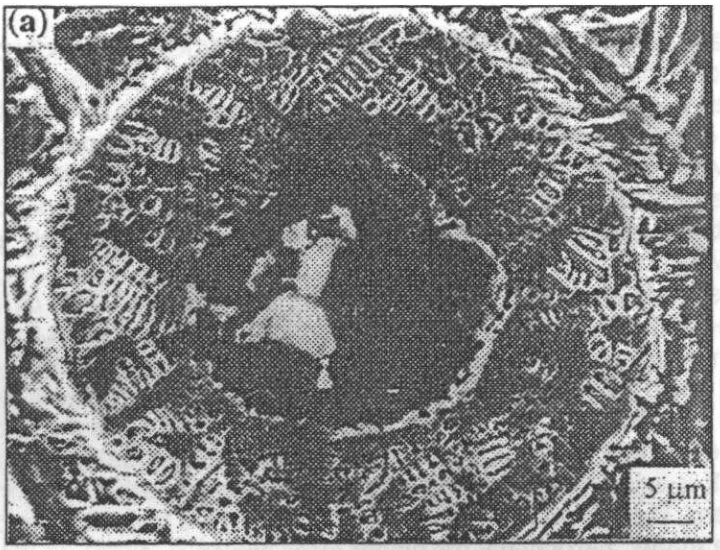

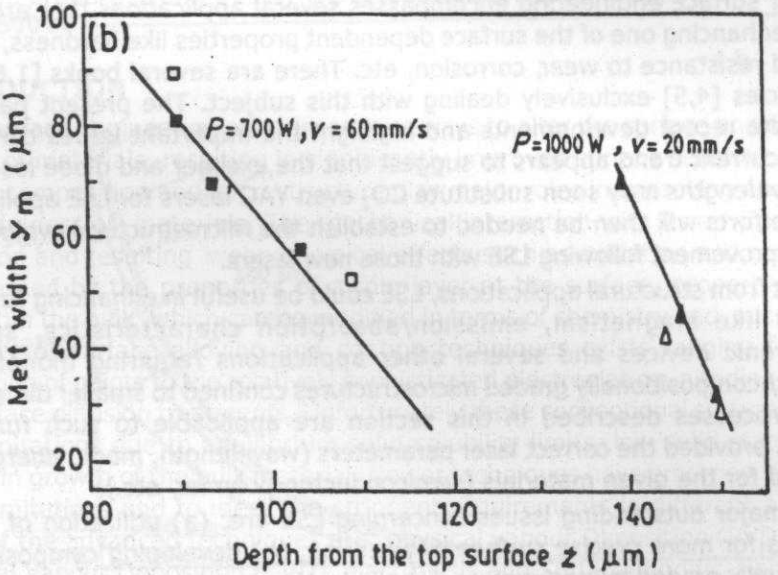

Fig. 16 : (a) Partial melting of a graphite nodule embedded in the ferritic/martensitic matrix following LSH with 650 W power and 60 mm/s scan speed. Note that melting initiated at the graphite-matrix interface and consumed nearly half the nodule from the circumference, and (b) variation of predicted melts widths (ym) around graphite nodules as a function of depth (z) from the surface. Open and solid symbols represent experimental and predicted data, respectively [51].

REFERENCES

1. P. A. Molian, Surface Modification Technologies-An Engineers Guide, (ed. T. S. Sudarshan), Marcel Dekker Inc., New York, (1989), p. 421.
2. W. W. Duley, Laser Surface Treatment of Metals, (eds. C. W. Draper and P. Mazzoldi) NATO-ASI Series (E) No.: 115, Martinus Nijhoff Publishers, Boston (1986), p. 3.
3. B. L. Mordike, Materials Science and Technology, (eds. R. W. Cahn, P. Haasen, E. J. Kramer), vol.15, VCH, Weinheim (1993), p. 111.
4. C. W. Draper and J. M. Poate, Inter. Met. Rev., 30 (1985) 85-108.
5. W. Draper and C. A. Ewing, J. Mater. Sci., 19 (1984) 3815.
6. W. M. Steen (ed.), Laser Material Processing, Springer Verlag, N. York, (1991).
7. C. W. Draper, Laser and Electron Beam Processing of Materials, (eds. C. W. White and P. S. Peercy), Academic Press, New York, (1980), p. 721.
8. C. W. White and M. J. Aziz, Surface Alloying by Ion, Electron and Laser Beams, (eds. L. E. Rehn, S. T. Picraux and H. Wiedersich), ASM, Metals Park, Ohio, (1987), p. 19.
9. S. T. Picraux and D. M. Follstaedt, Laser-Solid Interactions and Transient Thermal Processing of Materials (eds. J. Narayan, W. L. Brown and R. A. Lemons), North-Holland, New York, (1983), p. 751.
10. J. H. Perepezko and W. J. Boettinger, Surface Alloying by Ion, Electron and Laser Beams, (eds. L. E. Rehn, S. T. Picraux and H. Wiedersich), ASM, Metals Park, Ohio, (1987), p. 51.
11. B. L. Mordike, Materials Science and Technology, (eds. R. W. Cahn, P. Haasen, E. J. Kramer), vol.15, VCH, Weinheim (1993), p. 111.
12. C. W. Draper, Laser and Electron Beam Processing of Materials, (eds. C. W. White and P. S. Peercy), Academic Press, New York, (1980), p. 721.
13. J. Mazumdar, Lasers for Materials Processing, (ed. M. Bass), North Holland Pub. Co., New York, (1983), p. 113.
14. D. Raybould, M. Meola, R. Bye and S. K. Das, Mater. Sci. Eng. A, 241 (1998) 191-201.
15. A. Conde, I. Garcia and J. J. Damborenea, Corr. Sci., 43 (2001) 817-828.
16. C. T. Kwok, F. T. Cheng and H. C. Man, Surf. Coat. Tech., 145 (2001) 206-214.
17. L. W. Tsay, T. Y. Yang and M. C. Young, Mater. Sci. Eng. A, 311 (2001) 64-73.
18. P. Peyre, C. Braham, J. Ledion, L. Berthe and R. Fabbro, J. Mater. Eng. Perform., 9 (2000) 656-662.
19. C. T. Kwok, F. T. Cheng and H. C. Man, Mater. Sci. Eng. A, 290 (2000) 74-88; and C. T. Kwok, F. T. Cheng and H. C. Man, Mater. Sci. Eng. A, 290 (2000) 55-73.
20. Y. Isshiki, J. Shi, H. Nakai and M. Hashimoto, Applied Physics, A70 (2000) 651-656; and Y. Isshiki, J. Shi, H. Nakai and M. Hashimoto, Applied Physics, A70 (2000) 395-402.
21. J. Dutta Majumdar and I. Manna, Mater. Sci. Eng. A, 267 (1999) 50-59.
22. S. R. Pillai, P. Shankar, R. V. Subba-Rao, N. B. Sivai and S. Kumaravel, Mater. Sci. Tech., 17 (2001) 1249-1252.
23. P. Psyllaki and R. Oltra, Mater. Sci. Eng. A, 282 (2000) 145-152.
24. A. Agarwal, L. R. Katipelli and N. B. Dahotre, Metal. Mater. Trans. A, 31 (2000) 461-473.
25. F. T. Cheng, C. T. Kwok and H. C. Man, Surf. Coat. Tech., 139 (2001) 14-24.
26. X. L. Wu and Y. S. Hong, Metal. Mater. Trans. A, 31(2000) 3123-3127.
27. A. Roy and I. Manna, Mater. Sci. Eng. A297 (2001) 85-93.
28. A. Agarwal and N. B. Dahotre, Wear, 240 (2000) 144-151; and A. Agarwal and N. B. Dahotre, Metal. & Mater. Trans. A, 31(2000) 401-408.
29. S. Tondu, T. Schnick, L. Pawlowski, B. Wielage, S. Steinhauser and L. Sabatier, Surf. Coat. Tech., 123 (2000) 247-251.
30. J. M. Pelletier, E. Sauger, Y. Gachon and A. B. Vannes, J. Mater. Sci., 34 (1999) 2955-2969.